DESIGN CONSIDERATIONS FOR HEAVILY- DOPED CRYOGENIC SCHOTTKY DIODE VARACTOR MULTIPLIERS

E. Schlecht, F. Maiwald, G. Chattopadhyay, S. Martin and I. Mehdi
Jet Propulsion Laboratory, California Institute of Technology
MS 168-314
4800 Oak Grove dr.
Pasadena, CA 91109
310-354-4887 - erichs@merlin.jpl.nasa.gov

Abstract.

Diode modeling for Schottky varactor frequency multipliers above 500 GHz is presented with special emphasis placed on simple models and fitted equations for rapid circuit design. Temperature- and doping-dependent mobility, resistivity and avalanche current multiplication and breakdown are presented. Next is a discussion of static junction current, including the effects of tunneling as well as thermionic emission. These results have been compared to detailed measurements made down to 80 K on diodes fabricated at JPL, followed by a discussion of the effect on multiplier efficiency. Finally, a simple model of current saturation in the undepleted active layer suitable for inclusion in harmonic balance simulators is derived.

The research described in this publication was carried out at the Jet Propulsion Laboratory, California Institute of Technology, under a contract with the National Aeronautics and Space Administration.

I Introduction.

As diode multipliers are applied to higher frequencies (here used to mean above 500 GHz) the frequency dependent effects that can often be neglected at lower frequencies become more important. These include current saturation, carrier inertia, and capacitance of the undepleted epitaxial region [1,2]. More accurate multiplier performance predictions benefit from including these effects in the models used. Furthermore, current and future space missions are being designed to operate the LO multiplier chains at lower temperatures, near 120 K for instance [3]. Again, for accurate modeling temperature effects must be considered. These include the effects on mobility, breakdown voltage, static I/V current and current saturation. To aid in the rapid design of multipliers at many different power levels and frequency ranges, it is desirable to have models which are easy to implement using simple equations, with a minimum of arduous calculation, maximizing the speed of analysis. Thus, the more advanced models should still be fairly simple, suggesting the use of fitted equations.

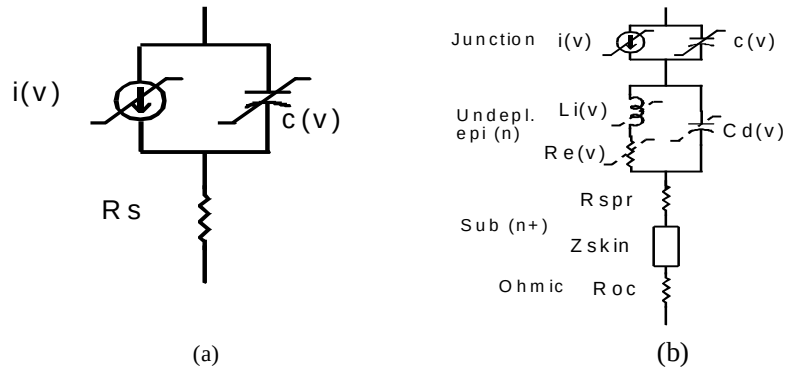

Figure 1. Diode circuit model. (a) Simplified. (b) More complete

As an illustration, Figure 1a shows a widely used diode model, which does a good job at lower frequencies, and can even work higher if well-calibrated. Figure 1b indicates the more sophisticated model discussed in this paper. The elements of the model will be investigated in the following sections. In section II the temperature-dependent material properties are discussed: mobility, resistivity, avalanche current multiplication and breakdown voltage. Section III is an analysis of the static junction current including the effects of tunneling, and its effect on multiplier efficiency. In section IV a simple model for analysis of current saturation in the undepleted epi region is introduced. The conclusions are presented in Section V.

II Diode Properties.

A. Mobility.

One of the primary loss mechanisms in the Schottky diode multiplier is signal absorption in the parasitic series resistance, depicted as R_s in Figure 1a and R_e, R_s, and R_{oc} in Figure 1b. The value of these resistances is proportional to the resistivities in the active epitaxial layer, the highly-doped sub-layer, and ohmic contacts respectively. Resistivity depends on the low field mobility, which can either be calculated by Monte Carlo methods [4-6] or measured [7, 8]. To facilitate calculation of the mobility for rapid design, a fitted algebraic equation is desired, including the effects of temperature and donor concentration. The author is not aware of a good fit, so the following expressions are suggested:

$$\mu = \left(\frac{1}{\mu_0} + \frac{1}{\mu_I} \right)^{-1} \tag{1}$$

$$\mu_0 = \frac{2296 \quad cm^2/Vs}{\left[\exp(490/T) - 0.42\right]^{-1} + (T/3410)^{1.3}} \tag{1a}$$

$$\mu_I = \frac{2.34\times10^5}{\left[\dfrac{1}{(184/T)^{2.3}+1} + \left(\dfrac{20}{T}\right)^{1.4}\right]\left[\dfrac{n_0}{10^{14}}\left(\dfrac{1+\theta}{1-\theta}\right)\right]^{0.86-T/900}} + \frac{10^4\left(e^{-\theta/0.68} - 0.27\right)}{T/163 + 0.8} \quad cm/Vs \tag{1b}$$

where T is the temperature in Kelvins, n_0 is the carrier concentration in cm^{-3}, and θ is the compensation ratio, defined [5] as the ratio of ionized acceptor to ionized donor concentrations. Since the normal donors in GaAs, such as Si, are shallow (~6 meV), as the carrier concentration increases the donor levels merge with the conduction band [9]. This occurs at a donor concentration of around 10^{16} cm^{-3}, and above that all donors are considered ionized except at extremely low temperatures, 10 K or so. Since the range of temperatures considered here is above 50 K and donor concentrations are above 10^{17} cm^{-3}, the carrier concentration is assumed equal to effective donor concentration, $N_D - N_A$, where N_D and N_A are the donor and acceptor concentrations.

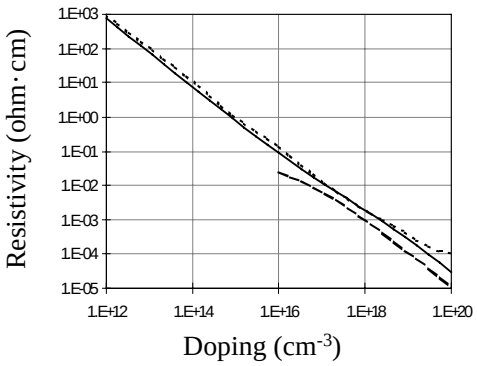

Figure 2. GaAs resistivity doping dependence. Solid line: 300 K calculation. Dotted line: From [10]. Broken line: 100K calculation.

The resistivity ρ is given by the usual formula:

$$1/\rho = q\mu n_0 \tag{2}$$

Figure 2 shows a plot of resistivity versus carrier concentration. Our room temperature and 100K calculations based on the formula above are compared to the room temperature plot in [10].

B. Avalanche current multiplication and breakdown.

Avalanche current multiplication caused by impact ionization is important in the reverse bias regime, especially for the highly doped diodes being used. This is the mechanism for junction breakdown, assuming the epi region is thicker than the depletion width when it occurs. Avalanche multiplication increases the current injected from one side of the depletion region by a factor M. Since impact ionization occurs at high fields, around 5×10^5 to 10^6 V/cm, it occurs first under the anode at high reverse bias, that is, the current being multiplied is comprised of electrons penetrating the barrier from the anode contact. Under these circumstances, M is given by [11]:

$$1 - \frac{1}{M} = \int_0^W \alpha_n \exp\left[-\int_0^{x'} (\alpha_n - \beta_p)\, dx' \right] dx \tag{3}$$

where α_n is the field-dependent electron ionization coefficient, β_p is the corresponding hole ionization coefficient, and W is the depletion width at the given voltage. To determine the breakdown voltage, M is taken to be infinite,

and the right side of (3) is solved iteratively to determine the applied voltage and corresponding field distribution and depletion width that make it unity.

Many researchers over the years have attempted to determine the ionization coefficients of GaAs [12-16]. For this work the measurements reported by Bulman et al. [14, 15] were used. Baraff [17] made calculations parameterizing the ionization coefficients at low temperature in terms of the optical phonon energy E_r, the mean free path between phonon scattering events λ, and the average ionization energy, E_i. These have been extended to all tempertures [18] using the assumption that E_i varies with temperature as the band gap energy and that E_r and λ vary as:

$$\frac{E_r}{E_{r0}} = \frac{\lambda}{\lambda_0} = \tanh\left(\frac{E_{r0}}{2kT}\right) \qquad \textbf{(4)}$$

where the zero subscripts refer to zero Kelvin values. The 0 K phonon energy is known to be 0.036 eV, so only values for E_i and λ_0 must be determined. The calculations in [17] have been fitted by Okuto and Crowell [18] to a simple formula. For our study the expression in [18] has been modified to fit Baraff's data more closely, which seems to model the measurements better. The modified equation is:

$$\alpha\lambda = f\sqrt{\frac{b}{x}}\exp\left[a - \sqrt{a^2 - x^2}\right] \qquad \textbf{(5)}$$

Here α is either α_n or β_p as appropriate, f is a simple factor which accounts both for variations in measurments and for the unknown ratio of impact ionization cross-section to phonon emission cross-section [17]. The expressions for a, b, and x are:

$$a = 0.116\left(\frac{E_i}{E_r}\right)^{1.266} \qquad b = 6.83\left(\frac{E_r}{E_i}\right) + 0.113 \qquad x = \frac{E_i}{qE\lambda} \qquad \textbf{(6,7,8)}$$

with E being the magnitude of the electric field. For this work values for the parameters that fit well to Bulman's data are: E_i = 2 eV and f = 0.44 for both electron and hole ionization coefficients, and λ_0 = 78.6 Å for α_n and 71.1 Å for β_p. As pointed out in [15, 19, 20] the ionization coefficients also depend on location. The effect of this was checked using the model of [15,20] , and it was found that for doping up to about 5×10^{17} the difference in breakdown voltage with and without this correction is only a few tens of millivolts.

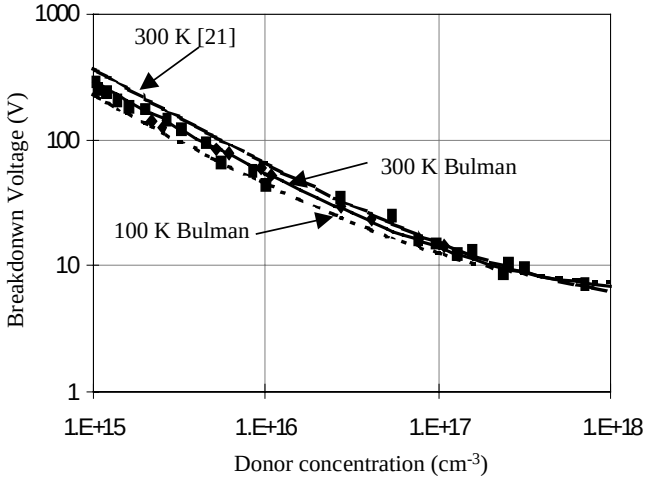

Figure 3. Breakdown voltage doping dependence. Scattered points represent measurements as described in text.

Figure 3 shows the breakdown voltage calculated using the ionization coefficients from equation (5) in equation (6) at 300 K, compared to a plot from [21] based on Pearsall's coefficients [13]. Also shown as scattered points are measurements used to derive the coefficients in [14,15] as well as others as reported in [22, 23]. The fit is better to those using Bulman's data at lower doping, although the difference between the two calculations is very small for the more highly doped diodes. Also shown is a curve indicating the breakdown voltage at 100 K calculated as above. Again, the temperature dependence is small at the higher dopings.

III Junction Current.

Quantum mechanical electron tunneling through the Schottky barrier is the dominant static current mechanism in low temperature and in highly doped diodes. This is because at high doping levels the depletion width is narrow, giving the large number of electrons below the top of the barrier a substantial probablity of tunneling through. At lower donor concentrations the depletion width is great enough that the dominant current mechanism is thermionic emission over the barrier. Several approximate tunneling current calculations were developed by Padovani and Stratton and others [24-27], but due to the approximations in calculating the tunneling coefficient the results are not valid over all current regimes. Recently the transfer matrix technique has been used [28, 29] to calculate the tunneling currents [30, 31]. This is a type of mode matching

algorithm wherein the barrier is divided up into a series of slices, each having a constant or linear potential profile. After the transmission coefficient, $T(E_n)$ is calculated for each value of the normal component of electron energy, E_n, the current density is calculated according to [32, equation (13)]. The transmission coefficient depends on the potential profile, including the barrier height, ϕ_b, which is given for an anode at $x = 0$ by:

$$\psi = \phi_b - qE_{\max} x\left(1-\frac{x}{W}\right) - \frac{q^2}{16\pi\varepsilon_r\varepsilon_0 x} \quad \textbf{(9)}$$

with $\varepsilon_r\varepsilon_0$ the semiconductor dielectric constant. The electric field under the anode is given as:

$$E_{\max} = \sqrt{\frac{2q(N_D - N_A)(\phi_b - V - V_n)}{\varepsilon_r\varepsilon_0}} \quad \textbf{(10)}$$

where V_n is the difference in potential between the Fermi level and the bottom of the conduction band in the semiconductor bulk. The barrier height itself commonly appears to have a dependence on the applied voltage [10, 33, 34]. For this work, the barrier height is characterized by an asymptotic "flat-band" height, Φ_{FB}, which is the barrier height at zero electric field, when the conduction bands would be flat. Additionally, the barrier height is assumed to have a linear dependence on E_{max}:

$$\phi_b = \Phi_{FB} - \alpha E_{\max} \quad \textbf{(11)}$$

Since E_{max} and ϕ_b, are mutually dependent, they must be solved for together as discussed in [33].

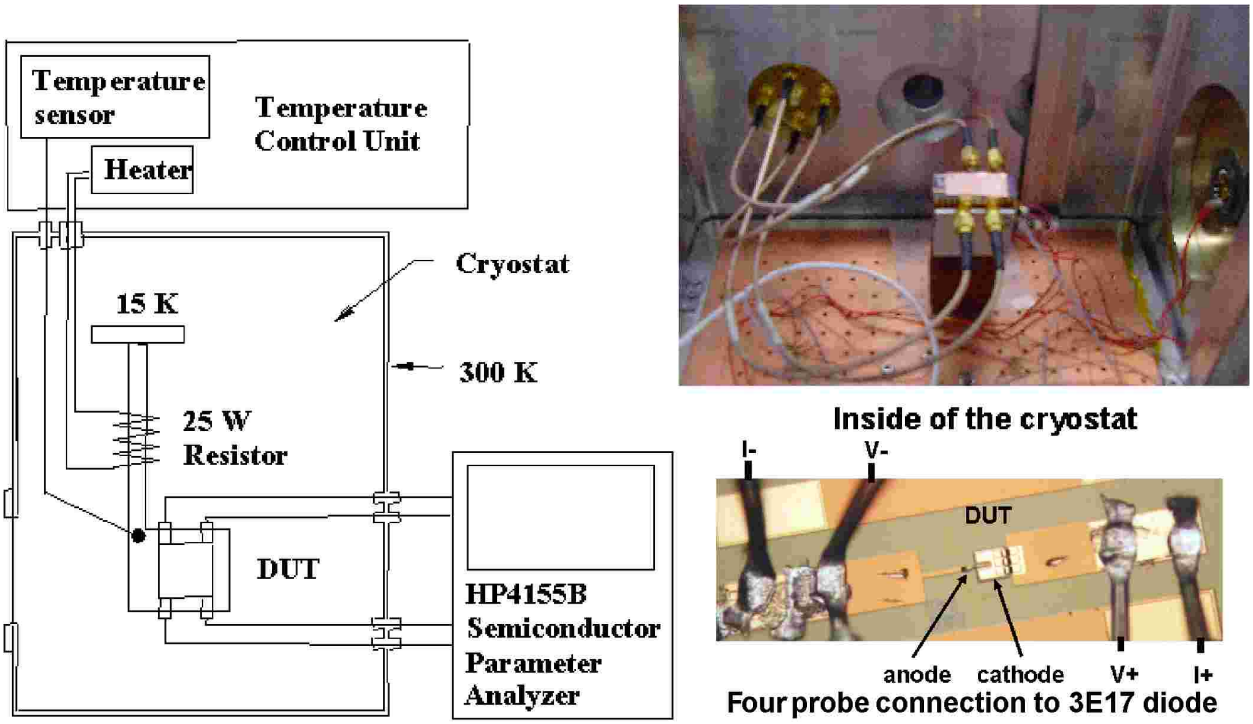

Figure 4. Block Diagram and photo of cryostat set up and wire-bonded diode.

To check the validity and determine the effect of the tunneling current on multiplier performance, several diodes fabricated at JPL have been measured over a wide temperature range in a specially designed cryostat [35]. The cryostat, shown in Figure 4, consists of a vacuum chamber enclosing the device under test (DUT) cooled by a two-stage closed-cycle Helium refrigerator. The temperature of the DUT is adjustable to within ±1 K in the 35-325 K range using a temperature controller with two temperature sensors, a 25 W heater and a bracket that mechanically connects the DUT to the 15 K second stage cold plate of the refrigerator.

The HP 4155B Semiconductor Parameter Analyzer is connected to the DUT with four cables for a four-probe measurement, compensating for the series resistance of the lines (Figure 2). Shielded cables connect the analyzer to SMA adaptors at the vacuum flange of the cryostat where the signals are fed through into the chamber. Inside the cryostat short sections of flexible cable connect the feed-through to the ceramic test socket which is

thermally bonded through a copper block to the temperature-stabilized cold plate. The diode is epoxied to the test socket and connected with four 25 μm bond wires to the carrier as also shown in Figure 4.

A diode fabricated a JPL on material doped to 3×10^{17} with an anode size of 1.5×10.5 μm^2 was measured from 100 to 300 K. The magnitude of the measured and calculated currents are compared in Figure 5. The current calculations included tunneling and avalanche multiplication as described earlier. Values of Φ_{FB} = 0.92 eV and α = 30 Å in equation (11) were used to fit the measurements. The fit is pretty good, but it is desirable to have independent justification for these values. The flat-band barrier height is dependent on the metal/semiconductor system in the contact. Using forward bias measurements of the reverse saturation current and ideality factor, the flat-band barrier height and effective barrier height, $\phi_{b,eff}$ can be determined as discussed in [36-39] based on the fact that as the applied voltage approaches the built-in voltage (flat-band), all current mechanisms except thermionic approach zero. This includes tunneling (because the bulk of electrons are near the barrier top in energy) and any models described by a linear field dependence (since the field approaches zero). This type of analysis was also performed on the above diode, with the results shown in Figure 6a. Since the JPL anodes are fabricated from Ti/Pt/Au, the flat-band barrier height should be compared to those metals. In [38] the reported heights are around 0.83 eV for Ti, 0.92 eV for Au and 0.99 eV for Pt. The measured values fit a line Φ_{FB} = 950–.3T meV, T being the temperature in Kelvin. It is possible that some intermixing may be taking place between the Ti and the Pt, but this cannot be said for certain. As to the α = 30 Å factor, many theories have been proposed explaining non-zero α as due to the imperfect nature of the metal-semiconductor interface [33, 34, 40-44]. Again, there is not enough data to pin this down.

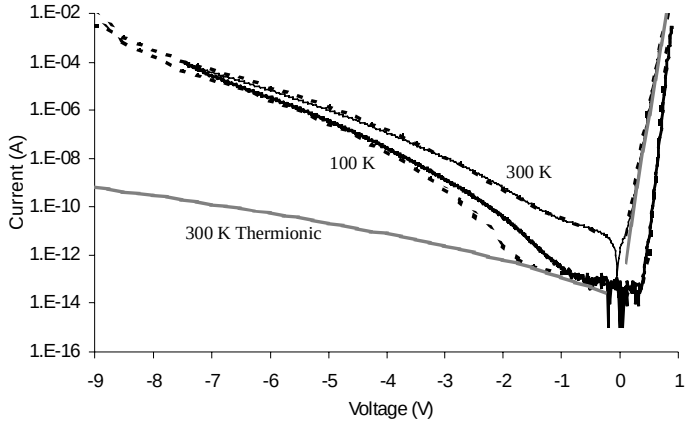

Figure 5. Tunneling/avalanche current calculations compared with measurement. The solid lines are measured currents, broken lines are calculated.

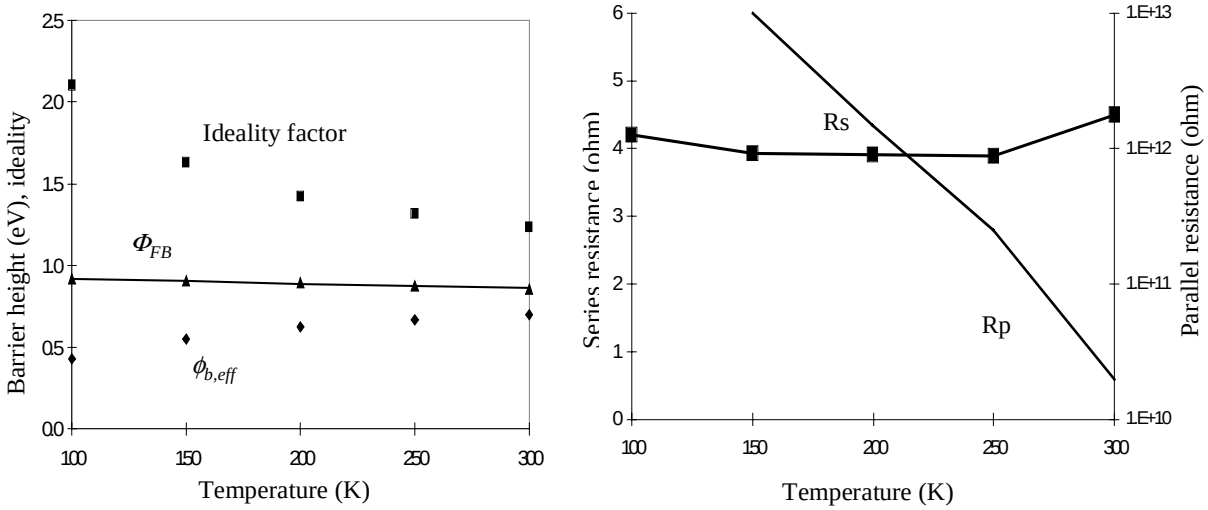

Figure 6. Characteristics of 3e17 diode. (a) Barrier height and ideality. The solid line is a model Φ_{FB} = 0.95-0.0003T eV. (b) Series and shunt resistances.

The series resistance and shunt resistance can also be found from the I/V data. These are plotted in Figure 6b. As expected, the series resistance R_s is independent of temperature (except for deviations ascribable to measurement uncertainty). The shunt resistance, R_p, however rises sharply at low temperatures. This is consistent

with a model wherein the shunt conduction is a surface "hopping" phenomenon, where the carriers do freeze out as the temperature drops. Generation-recombination current was considered, but it is proportional to the product of depletion width W and intrinsic carrier concentration n_i. For GaAs in general n_i is very low and for highly doped diodes W is small, so this current mechanism is insignificant in this case.

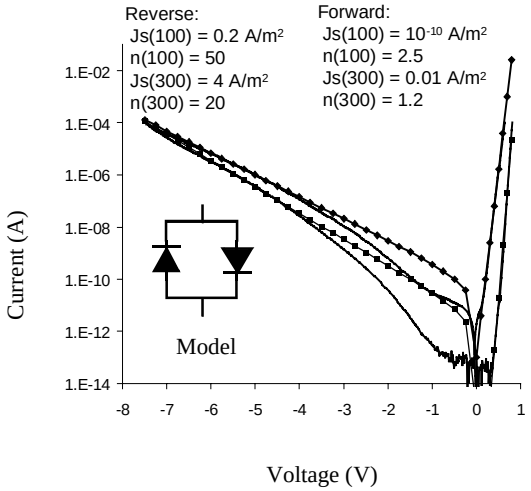

Figure 7. Fitted diode models and measurements, 100 & 300 K. Markers indicate fit models.

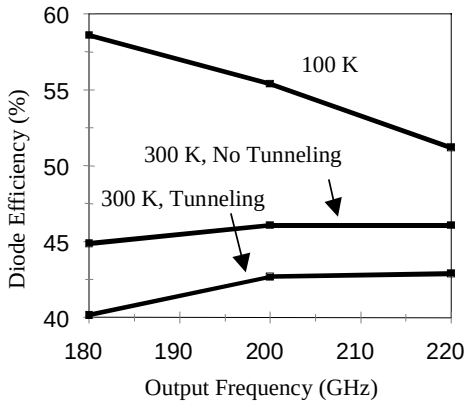

Figure 8. Efficiency of doubler with and without including tunneling current.

To evaluate the effect of these departures from thermionic behavior on multiplier efficiency, a simple model consisting of two diodes back-to-back was incorporated into a commercial harmonic balance simulator. A schematic is shown in Figure 7. One diode models the forward current, the other the reverse. The fit of the modeled current magnitude to the measurements is also shown in Figure 7. The fit is good for the forward bias, and not so good for reverse. However, the fit at the higher reverse currents is good, and the lower currents should have little effect on the performance of the multiplier.

Performance calculations of a 200 GHz multiplier with and without the reverse tunneling component are shown in Figure 8. As can be seen, at room temperature there is a significant reduction in efficiency when tunneling current is considered, but at 100 K there is no substantial difference. There is also no observed difference when the same calculation is performed at 800 GHz. These can be explained by noting that all Schottky multipliers suffer from two loss mechanisms: series resistance loss, which dominates, and conduction current loss. As the temperature is lowered, the conduction current drops (at a given voltage) so the conduction current contribution to the loss is greatly reduced. Hence, little difference in efficiency occurs with or without tunneling at low temperatures. At 800 GHz the efficiency is low and also greatly dominated by the series resistance loss, so the exact conduction current mechanism has little effect on efficiency.

IV Current Saturation.

As the electric field in a GaAs sample is increased, the velocity and hence the current reaches a peak, then begins to decline due to electrons gaining enough energy from the field to scatter into the upper, low-mobility valleys. This acts as a current limit in the undepleted epitaxial region of the diode. Current saturation reduces the efficiency of the diode as a multiplier because it decreases the ability of the charge at the edge of the depletion region to move around at the signal frequency and modulate the capacitance, generating the varactor non-linearity. There are also time constants associated with the transfer, and at the high frequencies being considered here they should be taken into account.

There are several equations used to describe the static current saturation profile. The simplest and oldest is the Kramer and Mircea formula [47]:

$$u(F) = \frac{\mu_0 F + u_s (F / F_N)^4}{1 + (F / F_N)^4} \qquad \textbf{(12)}$$

where u is the velocity, F the magnitude of the electric field, u_s the ultimate saturation velocity at about 20 kV/cm, and F_N is a characteristic field which determines where the peak velocity occurs. Usually current saturation, including transient effects have been modeled using Monte Carlo simulations (see, for example [45, 46]). Since

Monte Carlo calculations take large amounts of computer time, it is desirable to incorporate these effects into a harmonic balance (HB) circuit simulator using a simple model which can be integrated using the Runge-Kutta type integrators normally used in HB simulators. We propose to use a time constant based formulation somewhat similar to that introduced in [48]. The epi current is divided between two resistances representing the dominant two conduction band valleys in which electrons travel, as illustrated in Figure 9. Defining μ_0 as the lower valley mobility, (about 4000 cm^2/Vs or higher at reduced temperatures), and μ_1 is the upper valley mobility (about 400 cm^2/Vs) and n_0 and n_1 as the corresponding valley populations, the velocity in equation (12) can be written:

$$u(F) = \left(\mu_0 \frac{n_0}{n} + \mu_1 \frac{n_1}{n} \right) F \tag{13}$$

with n the total electron concentration in the undepleted epi. Then, several coupled differential equations are used to represent the time-dependent behavior of the velocity. The upper valley population is described by:

$$\frac{dn_1}{dt} = \frac{n_{1s}(V) - n_1(t)}{\tau} \tag{14}$$

where $n_{1s}(V)$ represents the static population of the upper valley, derived by combining equations (12) and (13) and noting that the total electron concentration is the sum of the populations of the two valleys, i.e. $n = n_0 + n_1$. The time constant, τ is dependent on the voltage across the epi, V_{tot}.

The current through the inductor representing carrier inertia has the usual equation:

$$\frac{di}{dt} = \frac{V_{tot}(t) - V(t)}{L_i} \tag{15}$$

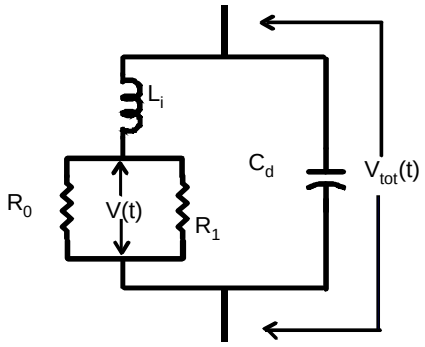

Figure 9. Simplified model of current saturation.

where L_i is the carrier inertia inductance, equal to:

$$L_i = \frac{m^* w}{q^2 n A} \tag{16}$$

with m^* the effective mass, w the thickness of the undepleted epi, and A the area of the diode. The total current through the inductance is simply:

$$i = qnuA \tag{17}$$

To simulate the full diode, of course, other equations must be included to model the epi capacitance, as well as the junction capacitance and conduction current.

As a check on the validity of the model, a test on a sample "undepleted epi" was made. It was assumed that this sample was of constant thickness, so that the equations above could be used, uncoupled from the epi capacitance, since the its current would depend on V_{tot} only, which is given as a boundary condition. In that case, equations (13) through (17) can be integrated using a numerical integrator with any given waveform for V_{tot}. In Figure 10 these calculations are compared with those in [46] for steps from zero electric field to the indicated values.

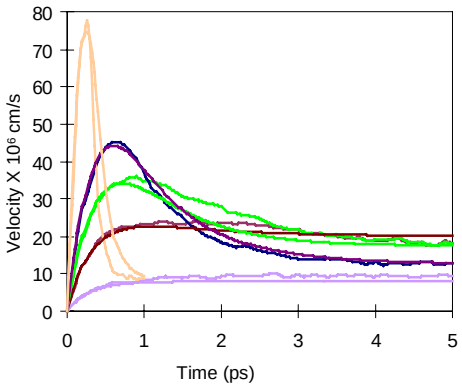

Figure 10. New current saturation model transient response (smooth curves) and results from [6] (rough curves).

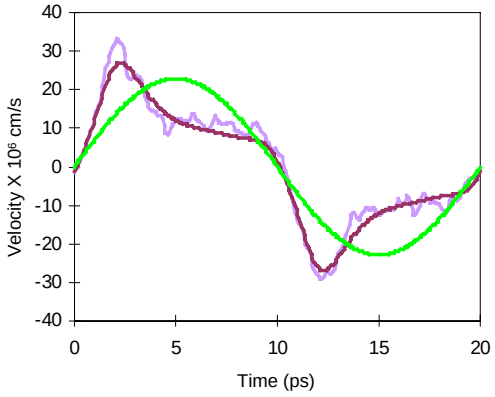

Figure 11. Sinusoidally pumped current saturation model (smooth line) compared to results from [46] (rough) and resistive approximation (sine wave).

It was found that values for τ ranging linearly from 0.2 ps at the 20 kV/cm to 3 ps at 1 kV/cm gave a good fit. As a further test, the same model is compared in Figure 11 with a sinusoidal 60 GHz excitation of 10 kV/cm amplitude. Again, the match is good. Also plotted is the current through a resistance having a mobility one-third that of GaAs (hence three times the resistance), which gives an estimate of the magnitude in performance reduction.

Currently, it appears that the above model, simple as it is, is impossible to incorporate into commercial HB simulators. Work is continuing in this direction, and a version of the Siegel/Kerr reflection algorithm HB simulator [49] is in progress so this model can be used to actually design multipliers.

V Conclusions.

Several suggestions have been made for improving the modeling of Schottky diodes for high doping and frequency, and low temperatures. The effects examined have been low-field mobility, breakdown, conduction current, barrier height and current saturation. Most of the effects serve to merely reduce the achievable efficiency, but not change the designs themselves very much, specifically the matching impedances. This is because the most important design parameter is the reactance tuning, dominated by the diode capacitance, which has been accurately modeled previously. However, the current saturation serves to greatly increase the effective series resistance, which is the dominant loss mechanism. It is possible to estimate the magnitude of the effect by using a series resistance much larger than the measured DC values in the performance estimates [50]. However, by calculating the behavior of current saturation with variations in doping and temperature, it should soon be possible to improve the optimization of the doping and anode sizes of high frequency multiplier diodes.

References

[1] T.W. Crowe, "GaAs Schottky Barrier Mixer Diodes for the Frequency Range 1-10 THz," Int. J. Infrared Millimeter Waves, vol. 10, no. 7, pp 765-777 (1989)

[2] J.T. Louhi and A.V. Räisänen, "On the Modeling and Optimization of Schottky Varactor Frequency Multipliers at Submillimeter Wavelengths," *IEEE Trans. Microwave Theory Tech*., vol. 43, no. 4, pp 922-926, 1995.

[3] N.D. Whyborn, "The HIFI Heterodyne Instrument for FIRST: Capabilities and Performance," in *Proc. ESA Symp. The Far Infrared and Submillimetre Universe 1997*, ESA-401.

[4] D.L Rode, "Low-Field Electron Transport," in *Semiconductors and Semimetals Volume 10*, ed. R.K. Willardson, and A.C. Beer, Academic Press, New York, 1975.

[5] W. Walukiewicz, L. Lagowski, L. Jastrzebski, M. Lichtensteiger, and H.C. Gatos, "Electron Mobility and Free-Carrier Absorption in GaAs: Determination of the Compensation Ratio," *J. Appl. Phys.* vol. 50, no. 2, pp 899-908, 1979.

[6] J.G. Ruch and W. Fawcett, "Temperature Dependence of the Transport Properties of Gallium Arsenide Determined by a Monte Carlo Method," *J. Appl. Phys.* vol. 41, no. 9, pp 3843-3849, 1970.

[7] G.E. Stillman, C.M. Wolfe, and J.O. Dimmock, "Hall Coefficient Factor for Polar Mode Scattering in n-Type GaAs," *J. Phys. Chem. Solids*, vol. 31, pp. 1199-1204, 1970.

[8] C.M. Wolfe, G.E. Stillman, and W.T. Lindley, "Electron Mobility in High-Purity GaAs," *J. Appl. Phys.*, vol. 41, no. 7, pp 3088-3091, 1970.

[9] G.E. Stillman, and C.M. Wolfe, "Electrical Characterization of Epitaxial Layers," *Thin Solid Films*, vol. 31, pp 69-88, 1976.

[10] S.M. Sze, *Physics of Semiconductor Devices*, 2nd Ed., Wiley, New York, 1981.

[11] G.E. Stillman, and C.M. Wolfe, "Avalanche Photodiodes," in *Semiconductors and Semimetals Volume 12*, ed. R.K. Willardson, and A.C. Beer, Academic Press, New York, 1977.

[12] R.A. Logan and S.M. Sze, "," J. Phys. Soc. Jap. Suppl., vol. 21, p 434, 1966.

[13] T.P. Pearsall, "The Band Structure Dependence of Impact Ionization by Hot Carriers in Semiconductors: GaAs," *Solid-State Electronics*, vol 21, pp 297-302, 1978.

[14] G.E. Bulman, V.M. Robbins, K.F. Brennan, K. Hess, and G.E. Stillman, "Experimental Determination of Impact Ionization Coefficients in (100) GaAs," *IEEE Electron Device Lettr.*, vol. EDL-4, no. 6, pp 181-185, 1983.

[15] G.E. Bulman, V.M. Robbins, and G.E. Stillman, "The Determination of Impact Ionization Coefficients in (100) Gallium Arsenide Using Avalanche Noise and Photocurrent Multiplication Measurements," IEEE Trans. Electron Devices, vol. ED-32, no. 11, pp 2454-2466, 1985.

[16] X.G. Zheng, P. Yuan, X. Sun, G.S. Kinsey, A.L, Holmes, B.G. Streetman, and J.C. Campbell, "Temperature Dependence of the Ionization Coefficients of AlxGa1-xAs," *IEEE J. Quantum Electr.*, vol. 36, no. 10, pp

1168-1173, 2000.
[17] G.A. Baraff, "Distribution Functions and Ionization Rates for Hot Electrons in Semiconductors," *Phys. Rev.*, vol. 128, no 6, pp. 2507-2517, 1962.
[18] Y. Okuto and C.R. Crowell, "Energy-Conservation Consideration in the Characterization of Impact Ionization in Semiconductors," *Phys. Rev. B*, vol. 6, no. 8, pp 3076-3081, 1972.
[19] Y. Okuto and C.R. Crowell, "Ionization Coefficients in Semiconductors: A nonlocalized Property," *Phys. Rev. B*, vol. 10, no. 10, pp. 4284-4296, 1974.
[20] Y. Okuto and C.R. Crowell, "Threshold Energy Effect on Avalanche Breakdown Voltage in Semiconductor Junctions," *Solid-State Electronics*, vol 18, pp 161-168, 1975.
[21] M.H. Lee and S.M. Sze, "Orientation Dependence of Breakdown Voltage in GaAs," *Solid-State Electronics*, vol 23, pp 1007-1009, 1980.
[22] B.J. Baliga, R. Ehle, J.R. Shealy and W. Garwacki, "Breakdown Characteristics of Gallium Arsenide," *IEEE Electron Device Lettr.*, vol. EDL-2, no. 11, pp 302-304, 1981.
[23] B.J. Baliga, A.R. Sears, P. Menditto and P.M. Campbell, "Extended Measurements of Gallium Arsenide Breakdown Characteristics Using Punchthrough Structures," *IEEE Electron Device Lettr.*, vol. EDL-5, no. 9, pp 385-387, 1984.
[24] F.A. Padovani and R. Stratton, "Field and Thermionic-Field Emission in Schottky Barriers," *Solid-State Electronics*, vol 9, pp 695-707, 1966.
[25] F.A. Padovani, "The Voltage-Current Characteristics of Metal-Semiconductor Contacts," in *Semiconductors and Semimetals Volume 7A*, ed. R.K. Willardson, and A.C. Beer, Academic Press, New York, 1971.
[26] C.R. Crowell and V.L. Rideout, "Normalized Thermionic-Field (T-F) Emission in Metal-Semiconductor (Schottky) Barriers," *Solid-State Electronics*, vol 12, pp 89-105, 1969.
[27] V.L. Rideout and C.R. Crowell, "Effects of Image Force and Tunneling on Current Transport in Metal-Semiconductor (Schottky Barrier) Contacts," *Solid-State Electronics*, vol 13, pp 993-1009, 1970.
[28] Y. Ando and T. Itoh, "Calculation of Transmission Tunneling Current Across Arbitrary Potential Barriers," *J. Appl. Phys.*, vol. 61, no. 4, pp. 1497-1502, 1987.
[29] W.W. Lui and M. Fukuma, "Exact Solution of the Schrodinger Equation Across and Arbitrary One-Dimensional Piecewise-Linear Potential Barrier," *J. Appl. Phys.*, vol. 60, no. 5, pp. 1555-1559, 1986.
[30] U.V. Bhapkar and R.J. Mattauch, "Numerical Simulation of the Current-Voltage Characteristics of Heteroepitaxial Schottky Barrier Diodes," *IEEE Trans. Electron Devices*, vol. 40, no. 6, 1993.
[31] J. Grajal, V. Krozer, E. González, F. Maldonado and J. Gismero, "Modeling and Design Aspects of Millimeter-Wave and Submillimeter-Wave Schottky Diode Varactor Frequency Multipliers," *IEEE Trans. Microwave Theory Tech.*, vol. 48, no. 4, 2000.
[32] R. Stratton, "Volt-Current Characteristics for Tunneling through Insulating Films," *J. Phys. Chem. Solids*, vol. 23, pp1177-1190, 1962.
[33] E.H. Rhoderick and R.H. Williams, *Metal-Semiconductor Contacts*, Second Edition, Oxford University Press, New York, 1988.
[34] J.M. Andrews and M.P. Lepselter, "Reverse Current-Voltage Characteristics of Metal-Silicide Schottky Diodes," *Solid-State Electronics*, vol 13, pp 1011-1023, 1970.
[35] Maestrini et. al, "Cryogenic operation of GaAs based multiplier chains to 400 GHz, " 8th Intl THz Conf, 2000.
[36] L.F. Wagner, R.W. Young and A. Sugerman, "A Note on the Correlation Between the Schottky-Diode Barrier Height and the Ideality Factor as Determined from I-V Measurements," *IEEE Electron Device Lettr.*, vol. 9 pp320-322, 1983.
[37] H.-W Hübers and H.P. Röser, "Temperature Dependence of the Barrier Height of Pt/n-GaAs Schottky Diodes," *J. Appl Phys.*, vol. 84, no. 9, pp 5326-5330, 1998.
[38] G. Myburg, F.D. Auret, W.E. Meyer, C.W. Louw and J.J. van Staden, "Summary of Schottky Barrier Height Data on Epitaxially Grown n- and p-GaAs," *Thin Solid Films*, vol. 325, pp181-186, 1998.
[39] V.W.L. Chin, M.A. Green and J.W.V. Storey, "Correlation Between Current-Voltage and Capacitance-Voltage Schottky Barrier Height on (100) and (110) GaAs and (110) InP Survaces," *J. Appl Phys.*, vol. 68, no. 7, pp 3470-3474, 1990.
[40] J. Tersoff, "Schottky Barriers and Semiconductor Band Structures," *Phys. Rev. B*, vol. 32, no. 10, pp 6968-6971, 1985.
[41] S.G. Louie, J.R. Chelikowsky and M.L. Cohen, "Ionicity and the Theory of Schottky Barriers," *Phys. Rev. B*, vol. 15, no. 4, pp 2154-2162, 1977.
[42] W. Mönch, "Barrier Heights of Real Schottky Contacts Explained by Metal-Induced Gap States and Lateral Inhomogeneities," *J. Vac. Sci. Technol. B*, vol. 17, no. 4, pp1867-1876, 1999.

[43] R.T. Tung, "Electron Transport at Metal-Semiconductor Interfaces: General Theory," *Phys. Rev. B*, vol. 45, no. 23, pp 13509-13523, 1992.
[44] R.T. Tung, "Chemical Bonding and Fermi Level Pinning at Metal-Semiconductor Interfaces," *Phys. Rev. Lettr*., vol. 84, no. 26., pp 6078-6081, 2000.
[45] T.J. Maloney and J. Frey, "Transient and Steady-State Electron Transport Properties of GaAs and InP," *J. Appl. Phys*., vol. 48, p 781, 1975.
[46] R.O. Grondin, P.A. Blakey, J.R. East, "Effects of Transient Carrier Transport in Millimeter-Wave GaAs Diodes," *IEEE. Trans. Electron Devices*, vol. ED-31, no. 1, pp 21-28, 1984.
[47] B. Kramer and A. Mircea, "Determination of Saturated Electron Velocity in GaAs," *Appl. Phys. Lettr*., vol. 26, no. 11, pp 623-625, 1975.
[48] D.E. McCumber and A.G. Chynoweth, "Theory of Negative-Conductance Amplification and of Gunn Instabilities in "Two-Valley" Semiconductors," *IEEE Trans. Electron Dev*., vol. ED-13, no. 1, pp 4-21, 1966.
[49] Siegel/Kerr NASA report, 1984.
[50] N.R. Erickson, private communicaion.